CHAPTER

Robust stability of connected cruise controllers

8

Dávid Hajdu[a,c], **Jin I. Ge**[b], **Tamás Insperger**[a,c], **Gábor Orosz**[d]

[a]*Department of Applied Mechanics, Budapest University of Technology and Economics, Budapest, Hungary*

[b]*Department of Computing and Mathematical Sciences, California Institute of Technology, Pasadena, CA, United States*

[c]*MTA-BME Lendület Human Balancing Research Group, Budapest, Hungary*

[d]*Department of Mechanical Engineering, University of Michigan, Ann Arbor, MI, United States, and Department of Civil and Environmental Engineering, University of Michigan, Ann Arbor, MI, United States*

Chapter outline

1 Introduction

Over the past few decades, passenger vehicles have been equipped with more and more automation features in order to improve active safety, passenger comfort, and traffic throughput of the road transportation system. In particular, adaptive cruise control (ACC) was invented to alleviate human drivers from the constant burden of speed control [1]. While the influence of ACC is yet to be observed in real traffic due to its low penetration rate, theoretical studies have found that ACC-equipped vehicles may have limited benefits on traffic flow [2,3]. In particular, very high penetration of ACC vehicles is required to suppress speed fluctuations propagating through vehicle strings, as each ACC vehicle only responds to its immediate predecessor [4].

Stability, Control and Application of Time-Delay Systems. https://doi.org/10.1016/B978-0-12-814928-7.00008-1

In order to overcome such limitations, cooperative adaptive cruise control (CACC) was proposed, where a platoon of ACC vehicles utilizes vehicle-to-everything (V2X) communication to coordinate their behavior [5–8]. CACC has been shown to have the potential to improve fuel economy and traffic efficiency in both theoretical and experimental studies [9–12]. However, the application of CACC in the early stages of driving automation may be significantly limited by the requirement that all vehicles in a CACC platoon must be automated aside from having V2X communication devices [13,14]. In particular, as mentioned in Ref. [15], "at low market penetrations, ... the probability of consecutive vehicles being equipped is negligible." Given the relatively low cost of V2X devices compared with driving automation, it is desirable to exploit the benefits of V2X without being restricted by the penetration rate of automation. Thus, we need to consider a connected automated vehicle design that is able to utilize V2X information sent from human-driven vehicles ahead.

For the longitudinal control of such a connected automated vehicle design, we proposed the concept of connected cruise control (CCC) that exploits ad hoc V2X communication from multiple human-driven vehicles ahead [16]. Several theoretical studies have shown that connected cruise control is able to significantly improve active safety and fuel economy of the connected automated vehicle by providing head-to-tail string stability [17–20].

Since connected automated vehicle design relies on models of preceding vehicles, uncertainties in the models need to be considered to guarantee robust performance of the connected vehicle system. In Refs. [21–23], uncertainties of vehicle parameters in an automated platoon was considered and robust controllers were synthesized using the $\mathcal{H}_\infty$ framework. Some other methods were also used in Refs. [24–27] to discuss the effects of unmodeled dynamics, stochastic communication delay, and measurement noise. However, a systematic method is needed to guarantee robust string stability against uncertain parameters of the human drivers ahead, such as their reaction time delays and feedback gains. In particular, uncertainties in the time delays should be taken into account without using overly conservative approximations. Moreover, such analysis should allow flexible connectivity topology and scale well as the number of vehicles connected via V2X communication increases. Therefore, in this chapter, we use structured singular value analysis [28,29] to provide tight bounds which allow connected cruise controllers to be head-to-tail string stable, despite uncertainties in human car-following behavior. We demonstrate through case studies how this robust string stability may improve the performance of a connected automated vehicle among human-driven vehicles.

2 Modeling and control design with delays

In this section, we first model the car-following behavior of human-driven vehicles in nonemergency situations; see Fig. 1A. While many existing car-following models can be used to describe the longitudinal behavior of human-driven vehicles, the optimal velocity model has a very simple mathematical form and provides great physical intuitions. Thus, we choose this to model human-driven vehicles and also use it as a

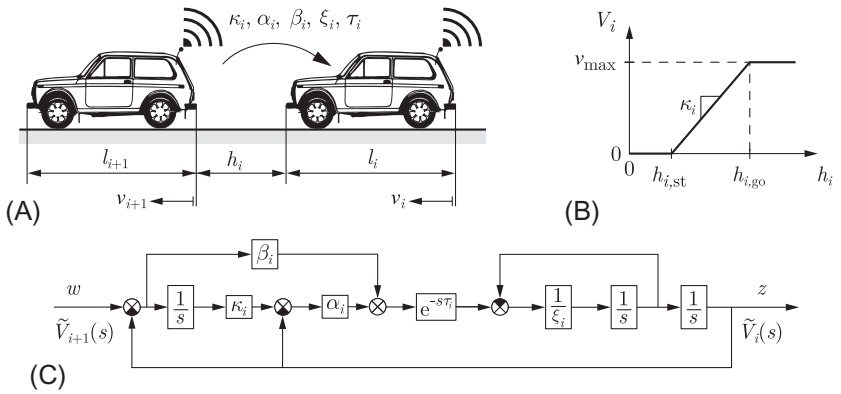

FIG. 1

Two-vehicle configuration: (A) car-following model; (B) range policy function $V_i(h_i)$ of vehicle i; and (C) block diagram of the transfer function $T_{i+1,i}(s)$ of vehicle i.

basis for connected vehicle controller. For both human car-following behavior and the connected cruise controller, we introduce the notion of plant and string stability and calculate the nominal stability regions without considering parameter uncertainty.

2.1 Car-following model

In this section, we introduce the model to describe the dynamics of a predecessor-follower pair. When neglecting the rolling resistance and air drag the longitudinal dynamics of the following vehicle i can be described by

$$\dot{h}_i(t) = v_{i+1}(t) - v_i(t), \tag{1}$$

$$\dot{v}_i(t) = a_i(t), \tag{2}$$

$$\dot{a}_i(t) = \frac{1}{\xi_i}(u_i(t) - a_i(t)), \tag{3}$$

where v_{i+1} is the velocity of the preceding vehicle, h_i, v_i, and a_i are the headway, velocity, and acceleration of the following vehicle i, and u_i is its acceleration command. The powertrain dynamics is modeled through the actuator lag ξ_i [16,30]. Since the follower only uses motion information from the immediate predecessor, the acceleration command can be described by

$$u_i(t) = \alpha_i(V_i(h_i(t-\tau_i)) - v_i(t-\tau_i)) + \beta_i(v_{i+1}(t-\tau_i) - v_i(t-\tau_i)), \tag{4}$$

where τ_i is the reaction time delay of a human driver and α_i and β_i are the control gains. Moreover, $V_i(h_i)$ is the range policy function that describes the desired velocity based on headway. Here, we consider

$$V_i(h_i) = \begin{cases} 0 & \text{if} \quad h_i \le h_{i,\mathrm{st}}, \\ \kappa_i(h_i - h_{i,\mathrm{st}}) & \text{if} \quad h_{i,\mathrm{st}} < h_i < h_{i,\mathrm{go}}, \\ v_{\max} & \text{if} \quad h_i \ge h_{i,\mathrm{go}}, \end{cases} \tag{5}$$

see Fig. 1B. That is, the desired velocity is zero for small headways ($h_i \leq h_{i,\mathrm{st}}$) and equal to the speed limit $v_{\max}$ for large headways ($h_i \geq h_{i,\mathrm{go}}$). Between these, the desired velocity increases with the headway linearly, with gradient κ_i. Note that when $h_{i,\mathrm{st}} = 0$ [m], $1/\kappa_i$ is often referred to as the time headway. Many other range policies may be chosen, but the qualitative dynamics remains similar if the earlier characteristics are kept.

Let us assume that the leader is traveling with the constant speed $v_{i+1}(t) \equiv v^*$, then the follower admits the equilibrium $h_i(t) \equiv h_i^*$, $v_i(t) \equiv v^*$, $a_i(t) \equiv 0$. We define the perturbations about the equilibrium as

$$\tilde{h}_i(t) = h_i(t) - h_i^*, \quad \tilde{v}_i(t) = v_i(t) - v^*, \quad \tilde{a}_i(t) = a_i(t), \tag{6}$$

that results in

$$\begin{aligned}
\dot{\tilde{h}}_i(t) &= \tilde{v}_{i+1}(t) - \tilde{v}_i(t), \\
\dot{\tilde{v}}_i(t) &= \tilde{a}_i(t), \\
\dot{\tilde{a}}_i(t) &= \frac{1}{\xi_i}(\alpha_i(\kappa_i \tilde{h}_i(t-\tau_i) - \tilde{v}_i(t-\tau_i)) + \beta_i(\tilde{v}_{i+1}(t-\tau_i) - \tilde{v}_i(t-\tau_i)) - \tilde{a}_i(t)).
\end{aligned} \tag{7}$$

Taking the Laplace transform of Eq. (7) with zero initial conditions, one may derive the transfer function

$$T_{i+1,i}(s) = \frac{\tilde{V}_i(s)}{\tilde{V}_{i+1}(s)} = \frac{(\alpha_i\kappa_i + \beta_i s)\mathrm{e}^{-s\tau_i}}{\xi_i s^3 + s^2 + (\alpha_i\kappa_i + (\alpha_i + \beta_i)s)\mathrm{e}^{-s\tau_i}}, \tag{8}$$

where s is the Laplace variable and $\tilde{V}_i(s)$ and $\tilde{V}_{i+1}(s)$ denote the Laplace transforms of $\tilde{v}_i(t)$ and $\tilde{v}_{i+1}(t)$. The block diagram is presented in Fig. 1C.

In the rest of Section 2.1, we assume nominal parameter values in Eq. (8) and discuss their influence in human car-following behaviors. By abuse of notation, we drop the indices i of parameters and refer to them as κ, α, β, τ, and ξ.

At the linear level, the system is *plant stable*, that is, approaches the equilibrium asymptotically, if all the infinitely many poles of Eq. (8), that is, the roots of the characteristic function

$$D(s) = \xi s^3 + s^2 + (\alpha\kappa + (\alpha + \beta)s)\mathrm{e}^{-s\tau} \tag{9}$$

are located on the left-half complex plane. When a real pole crosses the imaginary axis, substituting $s = 0$ into the characteristic equation $D(s) = 0$ yields the stability boundary

$$\alpha = 0. \tag{10}$$

On the other hand, when a complex conjugate pair of poles crosses the imaginary axis, substituting $s = \mathrm{i}\Omega$, $\Omega > 0$ into $D(s) = 0$ and separating the real and imaginary parts result in the stability boundary

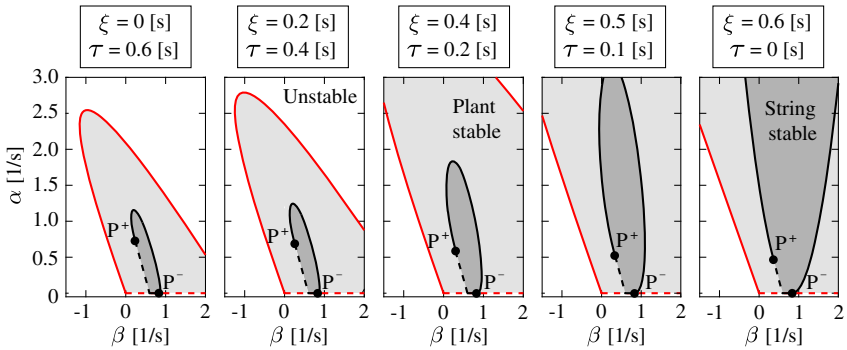

FIG. 2

Plant and string stability charts for different delays and lags, while fixing $\tau + \xi = 0.6$ [s], $\kappa = 0.6$ [1/s].

$$\alpha = \frac{\Omega^2}{\kappa}(\cos(\Omega\tau) - \xi\Omega\sin(\Omega\tau)), \tag{11}$$

$$\beta = \Omega(\xi\Omega\cos(\Omega\tau) + \sin(\Omega\tau)) - \alpha. \tag{12}$$

Stability diagrams are presented in Fig. 2, where the thick red curves (or gray in grayscale print) are the nominal plant stability boundaries and the shading indicates the domain of the plant-stable control gains. The sum of the time delay and lag is kept $\tau + \xi = 0.6$ [s], while having $\kappa = 0.6$ [1/s]. Comparison of the different panels reveals that the plant-stable domain decreases as the delay τ increases.

To ensure *string stability*, that is, the attenuation of velocity perturbations between the leader and the follower at the linear level, we consider sinusoidal excitation $\tilde{v}_{i+1}(t) = v_{i+1}^{\mathrm{amp}}\sin(\omega t)$, which (assuming plant stability) leads to the steady-state response $\tilde{v}_i^{\mathrm{ss}}(t) = v_i^{\mathrm{amp}}\sin(\omega t + \psi)$, where $v_i^{\mathrm{amp}}/v_{i+1}^{\mathrm{amp}} = |T_{i+1,i}(\mathrm{i}\omega)|$ and $\psi = \angle T_{i+1,i}(\mathrm{i}\omega)$. Requiring $|T_{i+1,i}(\mathrm{i}\omega)| < 1$ for all $\omega > 0$ ensures attenuation of sinusoidal signals and, as superposition holds for linear systems, for the linear combination of those signals. This condition may be rewritten as $\omega^2 P(\omega) > 0$ where

$$\begin{aligned} P(\omega) = {} & \alpha^2 + 2\alpha\beta + \omega^2 + \xi^2\omega^4 - 2(\alpha\kappa + (\alpha+\beta)\xi\omega^2)\cos(\omega\tau) \\ & - 2(\alpha + \beta - \alpha\kappa\xi)\omega\sin(\omega\tau). \end{aligned} \tag{13}$$

The stability boundaries can be identified corresponding to the minima of P becoming negative at $\hat{\omega} > 0$ that is defined by

$$P(\hat{\omega}) = 0, \tag{14}$$

$$\frac{\partial}{\partial\omega}P(\hat{\omega}) = 0, \tag{15}$$

while satisfying $\frac{\partial^2 P}{\partial^2 \omega}(\hat{\omega}) > 0$. Solving Eqs. (14), (15) for α and β one may obtain the string stability boundaries parameterized by $\hat{\omega}$ as

$$\alpha = f_1 \pm \sqrt{f_1^2 + 2f_0}, \tag{16}$$

$$\beta = \frac{\alpha\kappa(\xi\tau\hat{\omega}\cos(\hat{\omega}\tau) + (\xi+\tau)\sin(\hat{\omega}\tau)) + \hat{\omega}(1+2\xi^2\hat{\omega}^2)}{(2\xi+\tau)\hat{\omega}\cos(\hat{\omega}\tau) + (1-\xi\tau\hat{\omega}^2)\sin(\hat{\omega}\tau)} - \alpha, \tag{17}$$

where

$$f_0 = \frac{\hat{\omega}^2((1+(3\xi+\tau)\xi\hat{\omega}^2+\xi^3\tau\hat{\omega}^4)\sin(\hat{\omega}\tau) - \hat{\omega}(\tau-\xi^2(2\xi-\tau)\hat{\omega}^2)\cos(\hat{\omega}\tau))}{2(2\xi(\kappa\tau-1)-\tau)\hat{\omega}\cos(\hat{\omega}\tau) + 2(2\kappa(\xi+\tau)+\xi\tau\hat{\omega}^2-1)\sin(\hat{\omega}\tau)}, \tag{18}$$

$$f_1 = \frac{2\hat{\omega}(\kappa(\xi+\tau)-1+(\kappa\tau-2)\xi^2\hat{\omega}^2+\kappa_i\xi\cos(2\hat{\omega}\tau)) + \kappa(1-\xi^2\hat{\omega}^2)\sin(2\hat{\omega}\tau)}{2(2\xi(\kappa\tau-1)-\tau)\hat{\omega}\cos(\hat{\omega}\tau) + 2(2\kappa(\xi+\tau)+\xi\tau\hat{\omega}^2-1)\sin(\hat{\omega}\tau)}. \tag{19}$$

For $\hat{\omega} = 0$, the equalities $|T_{i+1,i}(0)| = 1$ and $\frac{\partial|T_{i+1,i}|}{\partial\omega}(0) = 0$ always hold. Thus, for string stability, we need $\frac{\partial^2|T_{i+1,i}|}{\partial\omega^2}(0) < 0$ which is equivalent to $P(0) = \alpha(\alpha+2\beta-2\kappa) > 0$. This gives the stability boundaries

$$\alpha = 0, \tag{20}$$

$$\alpha = 2(\kappa-\beta). \tag{21}$$

The nominal stability boundaries (16)–(21) are presented in Fig. 2 as black curves enclosing the string stable domain (shaded dark gray). Here, the dashed straight lines indicate the plant and string stability boundaries corresponding to $\Omega = 0$ and $\hat{\omega} = 0$, respectively. Note that the nominal string stable region grows and becomes open from above as τ decreases, indicating that the information delay τ has more significant influence on the string stability than the actuation lag ξ. Also, note that the string stable domain shrinks when the delay τ increases. In particular, there exist two anchor points P^+ and P^- corresponding to $\hat{\omega} = 0$,

$$(\alpha^+, \beta^+) = \left(\frac{4\kappa(\xi+\tau)-2}{2\tau(\kappa\tau-1)+\xi(4\kappa\tau-2)}, \frac{1-4\kappa(\xi+\tau)+2\kappa^2\tau(2\xi+\tau)}{2\tau(\kappa\tau-1)+\xi(4\kappa\tau-2)}\right), \tag{22}$$

$$(\alpha^-, \beta^-) = \left(0, \frac{1}{2(\xi+\tau)}\right), \tag{23}$$

which can be found by applying the L'Hospital rule to Eqs. (16)–(19). When increasing $\tau+\xi$ the anchor points move toward each other and when they meet, the string stable domain disappears. Using Eqs. (22), (23), we find the critical sum of the delay and lag is

$$\tau_{\text{cr}} + \xi_{\text{cr}} = \frac{1}{2\kappa}, \tag{24}$$

and for larger values the string stable domain disappears.

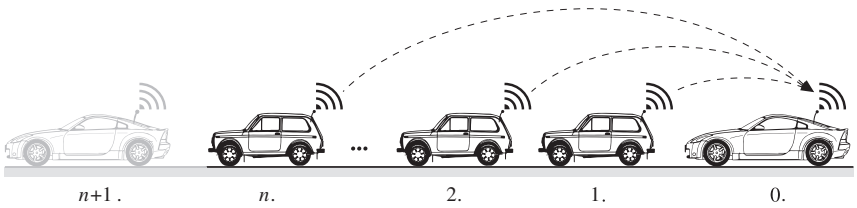

FIG. 3

A connected vehicle system resulting from a connected automated vehicle using V2X information from n human-driven vehicles ahead.

2.2 Connected vehicle systems

We consider a heterogeneous chain of vehicles where all vehicles are equipped with V2X communication devices and some are capable of automated driving, as shown in Fig. 3. When an automated vehicle receives motion information broadcasted from a few vehicles ahead, it may choose to use the information in its motion control (see the dashed arrows), and thus, it becomes a connected automated vehicle. Such a V2X-based controller then defines a connected vehicle system consisting of the connected automated vehicle and the preceding vehicles whose motion signals are used by the connected automated vehicle.

Inside this connected vehicle system, we denote the connected automated vehicle as vehicle 0, and the preceding vehicles as vehicles $1, \ldots, n$. Note that we assume a connected automated vehicle does not "look beyond" another connected automated vehicle. For example, in Fig. 3, vehicle 0 does not include the V2X signals from vehicles farther ahead than vehicle n in its controller. This assumption greatly simplifies the topology of connected vehicle systems and eliminates intersections of links that are typically detrimental for the performance of the system [17,31].

The connected cruise controller for the connected automated vehicle ($i = 0$) is assumed in the form of

$$u_0(t) = A_{1,0}(V_0(h_0(t-\sigma_{1,0})) - v_0(t-\sigma_{1,0})) + \sum_{j=1}^{n} B_{j,0}(v_j(t-\sigma_{j,0}) - v_0(t-\sigma_{j,0})), \quad (25)$$

where the control gains $A_{j,0}$ and $B_{j,0}$ and communication delay $\sigma_{j,0}$ correspond to the links between vehicle j and the connected automated vehicle 0. Here, the range policy function $V_0(h_0)$ is defined as in Eq. (5), and its gradient is denoted by κ_0 for $h_{0,\mathrm{st}} \le h_0 \le h_{0,\mathrm{go}}$.

Unlike many CACC algorithms, in the connected vehicle system shown in Fig. 3, the preceding vehicles $1, \ldots, n$ are not required to cooperate with the connected automated vehicle. Moreover, aside from broadcasting their motion information through V2X communication, no automation of these vehicles is required. Correspondingly,

the feedback gains and delay times in Eq. (4) cannot be tuned for the connected automated vehicle design. However, the connected automated vehicle 0 may fully exploit V2X signals from vehicles $1, \ldots, n$ with no constraint on the connectivity topology.

Note that when $n = 1$, the connected automated vehicle only uses motion information from its immediate predecessor, and Eq. (25) gracefully degrades to the same control structure as human-driven vehicles [32] or automated vehicles without connectivity [4].

Similarly as in Section 2.1, here we consider the nominal stability of the connected vehicle system (1)–(4), (25) around the equilibrium, where the vehicles travel with the same constant speed $v_i(t) = v^*$, $a_i(t) = 0$ and their corresponding headways are constant $h_i(t) = h_i^*$ such that $V_i(h_i^*) = v^*$. Linearization of Eqs. (1)–(4) including Eq. (25) about the equilibrium $(h_i^*, v^*, 0)$ gives

$$\begin{aligned}
\dot{\tilde{h}}_0(t) &= \tilde{v}_1(t) - \tilde{v}_0(t), \\
\dot{\tilde{v}}_0(t) &= \tilde{a}_0(t), \\
\dot{\tilde{a}}_0(t) &= \frac{1}{\xi_0}\Bigg(A_{1,0}(\kappa_0 \tilde{h}_0(t-\sigma_{1,0}) - \tilde{v}_0(t-\sigma_{1,0})) \\
&\qquad + \sum_{i=1}^{n} B_{i,0}(\tilde{v}_i(t-\sigma_{i,0}) - \tilde{v}_0(t-\sigma_{i,0})) - \tilde{a}_0(t)\Bigg)
\end{aligned} \tag{26}$$

for the connected automated vehicle and

$$\begin{aligned}
\dot{\tilde{h}}_i(t) &= \tilde{v}_{i+1}(t) - \tilde{v}_i(t), \\
\dot{\tilde{v}}_i(t) &= \tilde{a}_i(t), \\
\dot{\tilde{a}}_i(t) &= \frac{1}{\xi_i}(\alpha_i(\kappa_i \tilde{h}_i(t-\tau_i) - \tilde{v}_i(t-\tau_i)) + \beta_i(\tilde{v}_{i+1}(t-\tau_i) - \tilde{v}_i(t-\tau_i)) - \tilde{a}_i(t))
\end{aligned} \tag{27}$$

for the human-driven vehicles $i = 1, \ldots, n$.

We assume that the connected vehicle system (26), (27) is plant stable, that is, when the input perturbation $\tilde{v}_{n+1}(t) \equiv 0$, the perturbations $\tilde{h}_i$, $\tilde{v}_i$, $\tilde{a}_i$ of the preceding vehicles and $\tilde{h}_0$, $\tilde{v}_0$, $\tilde{a}_0$ of the connected automated vehicle tend to zero regardless of the initial conditions. Instead, we focus on how the connected automated vehicle responds to speed perturbations propagating through the system. When the speed fluctuation $\tilde{v}_0$ of the connected automated vehicle has smaller amplitude than the input $\tilde{v}_n$, we call the connected automated vehicle design head-to-tail string stable.

The notion of string stability between two consecutive vehicles was previously used to explain the amplification of speed perturbations along a chain of vehicles without connectivity [33]. However, by considering head-to-tail string stability, we allow speed perturbations to be amplified among the uncontrollable vehicles $1, \ldots, n$, and we focus on how the connected automated vehicle attenuates the perturbations.

Being head-to-tail string stable not only enables a connected automated vehicle to enjoy better active safety, energy efficiency, and passenger comfort, but also it can help to mitigate traffic waves [17].

We assume zero initial conditions for Eqs. (26), (27) and obtain

$$\begin{aligned} \tilde{V}_0(s) &= \sum_{i=1}^{n} T_{i,0}(s)\tilde{V}_i(s), \\ \tilde{V}_i(s) &= T_{i+1,i}(s)\tilde{V}_{i+1}(s), \end{aligned} \tag{28}$$

where $\tilde{V}_0(s)$ and $\tilde{V}_i(s)$ denote the Laplace transforms of $\tilde{v}_0(t)$ and $\tilde{v}_i(t)$, and the link transfer functions are

$$T_{1,0}(s) = \frac{(A_{1,0}\kappa_0 + B_{1,0}s)\mathrm{e}^{-s\sigma_{1,0}}}{\xi_0 s^3 + s^2 + A_{1,0}(\kappa_0 + s)\mathrm{e}^{-s\sigma_{1,0}} + \sum_{l=1}^{n} B_{l,0}s\mathrm{e}^{-s\sigma_{l,0}}}, \tag{29}$$

$$T_{i,0}(s) = \frac{B_{i,0}s\mathrm{e}^{-s\sigma_{i,0}}}{\xi_0 s^3 + s^2 + A_{1,0}(\kappa_0 + s)\mathrm{e}^{-s\sigma_{1,0}} + \sum_{l=1}^{n} B_{l,0}s\mathrm{e}^{-s\sigma_{l,0}}}, \tag{30}$$

$$T_{i+1,i}(s) = \frac{(\alpha_i\kappa_i + \beta_i s)\mathrm{e}^{-s\tau_i}}{\xi_i s^3 + s^2 + (\alpha_i\kappa_i + (\alpha_i + \beta_i)s)\mathrm{e}^{-s\tau_i}}. \tag{31}$$

Thus, the head-to-tail transfer function of the connected vehicle system is

$$G_{n,0}(s) = \frac{\tilde{V}_0(s)}{\tilde{V}_n(s)} = \det(\mathbf{T}(s)), \tag{32}$$

where the transfer function matrix is given by

$$\mathbf{T}(s) = \begin{bmatrix} T_{1,0}(s) & -1 & 0 & \cdots & 0 & 0 \\ T_{2,0}(s) & T_{2,1}(s) & -1 & \cdots & 0 & 0 \\ T_{3,0}(s) & 0 & T_{3,2}(s) & \cdots & 0 & 0 \\ \vdots & \vdots & \vdots & \ddots & \vdots & \vdots \\ T_{n-1,0}(s) & 0 & 0 & \cdots & T_{n-1,n-2}(s) & -1 \\ T_{n,0}(s) & 0 & 0 & \cdots & 0 & T_{n,n-1}(s) \end{bmatrix}, \tag{33}$$

see Ref. [17] for the proof. The criterion for head-to-tail string stability at the linear level is guaranteed if the perturbations are attenuated for any frequency, that is,

$$|\det(\mathbf{T}(\mathrm{i}\omega))| < 1, \quad \forall\omega > 0, \tag{34}$$

where we substituted $s = \mathrm{i}\omega$. In order to facilitate robustness analysis in the following section, we rewrite Eq. (34) as

$$1 - \det(\mathbf{T}(\mathrm{i}\omega))\delta^{\mathrm{c}} \neq 0, \quad \forall\omega > 0, \tag{35}$$

where δ^{c} is an arbitrary complex number inside the unit circle in the complex plane, that is, $\delta^{\mathrm{c}} \in \mathbb{C}$, $|\delta^{\mathrm{c}}| < 1$.

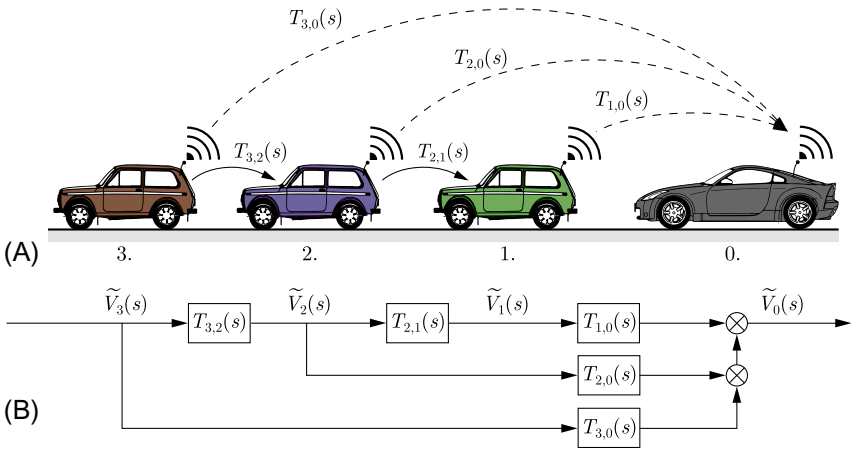

FIG. 4

A four-vehicle configuration: (A) connected vehicle system with the information flow indicated by the *dashed arrows* and (B) the corresponding block diagram showing the propagation of speed perturbations $\tilde{V}_i(s)$, for $i = 3, 2, 1, 0$.

To illustrate the head-to-tail string stability, here we consider a connected automated vehicle using motion information from three preceding vehicles, as shown in Fig. 4A. The transfer function matrix for this connected vehicle system is

$$\mathbf{T}(s) = \begin{bmatrix} T_{1,0}(s) & -1 & 0 \\ T_{2,0}(s) & T_{2,1}(s) & -1 \\ T_{3,0}(s) & 0 & T_{3,2}(s) \end{bmatrix}, \tag{36}$$

where the elements $T_{1,0}(s)$, $T_{2,0}(s)$, $T_{3,0}(s)$, $T_{2,1}(s)$, and $T_{3,2}(s)$ are given by Eqs. (29)–(31), while Eq. (32) results in the head-to-tail transfer function

$$G_{3,0}(s) = \det(\mathbf{T}(s)) = T_{3,0}(s) + T_{3,2}(s)T_{2,0}(s) + T_{3,2}(s)T_{2,1}(s)T_{1,0}(s). \tag{37}$$

The flow of information is illustrated on a schematic block diagram in Fig. 4B. We consider the case when the preceding vehicles $i = 1, 2$ have parameters $\alpha_i = 0.25$ [1/s], $\beta_i = 0.5$ [1/s], $\kappa_i = 0.8$ [1/s], $\tau_i = 0.3$ [s], $\xi_i = 0.5$ [s], while the connected automated vehicle has $\sigma_{1,0} = \sigma_{2,0} = \sigma_{3,0} = \sigma = 0.1$ [s], $\kappa_0 = 0.6$ [1/s], $\xi_0 = 0.5$ [s] and the design parameters are chosen as $A_{1,0} = 0.4$ [1/s], $B_{1,0} = 0.2$ [1/s], $B_{2,0} = 0.4$ [1/s], and $B_{3,0} = 0.4$ [1/s].

In Fig. 5A, we plot the head-to-tail transfer function $|G_{3,0}(\mathrm{i}\omega)|$ of the connected automated vehicle (solid gray curve) and the link transfer function $|T_{3,2}(\mathrm{i}\omega)|$ that describes how vehicle 2 responds to the motion of vehicle 3 (dotted purple curve). Here this is equal to $|T_{2,1}(\mathrm{i}\omega)|$ as vehicles 2 and 1 have the same parameters. While the magnitude of the head-to-tail transfer function stays below 1, the link transfer functions of vehicles 2 and 1 reach beyond 1 for low frequencies. This indicates that

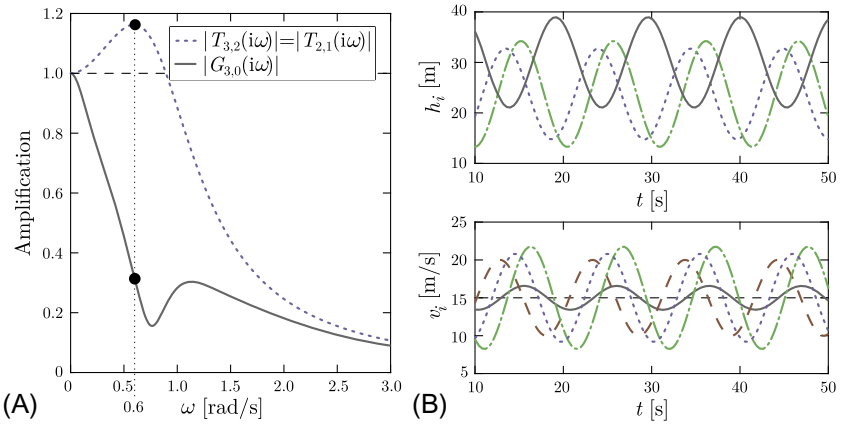

FIG. 5

(A) Example transfer functions $|T_{3,2}(\mathrm{i}\omega)| = |T_{2,1}(\mathrm{i}\omega)|$, $|G_{3,0}(\mathrm{i}\omega)|$ and (B) corresponding simulations for $\omega = 0.6\,[\mathrm{rad/s}]$.

speed perturbations at low frequency are amplified by vehicles 2 and 1 but eventually are suppressed by the connected automated vehicle. This observation is supported by a simulation shown in Fig. 5B, where the speed input $v_3(t) = v^* + v_3^{\mathrm{amp}} \sin(\omega t)$ with $v^* = 15\,[\mathrm{m/s}]$, $v_3^{\mathrm{amp}} = 5\,[\mathrm{m/s}]$, $\omega = 0.6\,[\mathrm{rad/s}]$ is plotted as dashed brown curve. The stationary time profiles for vehicles 2 and 1 are plotted by dotted purple and point-dotted green curves, respectively. The color code corresponds to the vehicle colors in Fig. 4A.

In Fig. 5B, one may notice the difference in the equilibrium headway, that is, $h_0^* = 30\,[\mathrm{m}]$ and $h_1^* = h_2^* = 23.75\,[\mathrm{m}]$. This is caused by the differences in the slopes of the range policy functions $V_i(h_i)$. In particular, while $h_{i,\mathrm{st}} = 5\,[\mathrm{m}]$ for $i = 0, 1, 2$, we have $\kappa_0 = 0.6\,[1/\mathrm{s}]$ and $\kappa_1 = \kappa_2 = 0.8\,[1/\mathrm{s}]$; see Eq. (5) and Fig. 1B. This highlights that the trajectories in Fig. 5B strongly depend on the parameters of the preceding vehicles. The same control parameters used in Fig. 5 may behave poorly with a different set of parameters κ_i, α_i, β_i, τ_i, and ξ_i.

3 Robust string stability

Since a connected automated vehicle may not know the dynamics of the preceding vehicles $1, \ldots, n$ accurately, the V2X-based controller should be robust against their parameter uncertainties (aside from the model uncertainties of the connected automated vehicle itself). In this section, we assume additive perturbations $\tilde{\kappa}_i$, $\tilde{\alpha}_i$, $\tilde{\beta}_i$, $\tilde{\tau}_i$, and $\tilde{\xi}_i$ in the parameters of human-driven vehicles. To ensure good performance under these parameter changes, we apply robust control design.

3.1 Uncertainties in a predecessor-follower system

As an illustration of the robust string stability, we consider vehicle i that only uses information from one vehicle ahead. Here, we set $i = 0$ without loss of generality (see Fig. 1) and drop the index i of the parameters κ, α, β, τ, and ξ in this section. Thus, we have the input $\tilde{v}_{i+1}(t)$, the output $\tilde{v}_i(t)$, and the nominal head-to-tail transfer function is given by

$$G_{i+1,i}(s) = T_{i+1,i}(s) = \frac{(\alpha\kappa + \beta s)\mathrm{e}^{-s\tau}}{\xi s^3 + s^2 + (\alpha\kappa + (\alpha + \beta)s)\mathrm{e}^{-s\tau}}, \tag{38}$$

see Eq. (8).

Uncertainties in the plant may appear in different forms. Without any restrictions, let us assume that every parameter in the model is uncertain. While additive uncertainties $\tilde{\alpha}$, $\tilde{\beta}$, $\tilde{\xi}$, and $\tilde{\kappa}$ result in additive uncertainty terms, an additive delay uncertainty $\tilde{\tau}$ will result in a multiplicative exponential term $\mathrm{e}^{-s\tilde{\tau}}$ in Eq. (38), that is,

$$G_{i+1,i}(s) + \tilde{G}_{i+1,i}(s) = \frac{((\kappa + \tilde{\kappa})(\alpha + \tilde{\alpha}) + (\beta + \tilde{\beta})s)\mathrm{e}^{-s(\tau+\tilde{\tau})}}{(\xi + \tilde{\xi})s^3 + s^2 + ((\kappa + \tilde{\kappa})(\alpha + \tilde{\alpha}) + (\alpha + \tilde{\alpha} + \beta + \tilde{\beta})s)\mathrm{e}^{-s(\tau+\tilde{\tau})}}, \tag{39}$$

where $\tilde{G}_{i+1,i}(s)$ represents only the uncertainty. In spite of the fact that $\tilde{G}_{i+1,i}(s)$ can be expressed algebraically, the question is how to formulate the uncertain model that is the most suitable for robust analysis.

In order to formulate the uncertainties in a general way, we must separate the uncertainty from the nominal model. We use the Rekasius substitution to handle uncertainty in the delay, such that

$$\mathrm{e}^{-s\tilde{\tau}} = \frac{1 - s\tilde{\vartheta}(s)}{1 + s\tilde{\vartheta}(s)}, \tag{40}$$

where we restrict ourselves to $s = \mathrm{i}\omega$ and therefore, we have

$$\tilde{\vartheta}(\mathrm{i}\omega) = \frac{1}{\omega}\tan\frac{\omega\tilde{\tau}}{2}, \tag{41}$$

see Ref. [34]. This substitution is exact and suitable for the robust analysis in the region $0 \leq \omega < \pi/\tilde{\tau}$, since it covers the same domain in the complex plane as $\mathrm{e}^{-\mathrm{i}\omega\tilde{\tau}}$. Similar attempt with higher-order approximation is given in Ref. [35].

By taking into account the uncertain parameters (with the Rekasius substitution), the block diagram shown in Fig. 6 can be drawn. Based on this graphical representation, one can get the following system of equations for the inputs $\mathbf{u} = [u_1, u_2, u_3, u_4, u_5]^\top$, $w = \tilde{V}_{i+1}(s)$ and outputs $\mathbf{y} = [y_1, y_2, y_3, y_4, y_5]^\top$, $z = \tilde{V}_i(s)$ in the form

$$y_1 = (w - z)\frac{1}{s}, \tag{42}$$

$$y_2 = (w - z)\frac{1}{s}\kappa + u_1 - z, \tag{43}$$

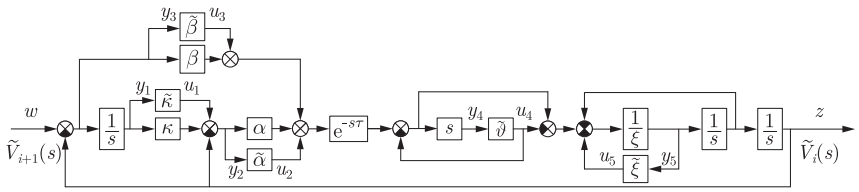

FIG. 6

Block diagram of the car-following model with parametric uncertainty.

$$y_3 = (w - z), \tag{44}$$

$$y_4 = \left(\left(\left((w-z)\frac{1}{s}\kappa + u_1 - z\right)\alpha + u_2 + u_3 + (w-z)\beta\right)\mathrm{e}^{-s\tau} - u_4\right)s, \tag{45}$$

$$y_5 = \left(\frac{y_4}{s} - u_4 - u_5 - y_5\frac{1}{s}\right)\frac{1}{\xi}, \tag{46}$$

$$z = y_5\frac{1}{s}\frac{1}{s}. \tag{47}$$

This can be formulated as

$$\begin{bmatrix}\mathbf{y}\\ z\end{bmatrix} = \mathbf{m}(s)\begin{bmatrix}\mathbf{u}\\ w\end{bmatrix}, \tag{48}$$

$$\mathbf{u} = \boldsymbol{\delta}(s)\mathbf{y}, \tag{49}$$

where $\mathbf{m}(s)$ is the interconnection matrix and $\boldsymbol{\delta}(s)$ is the uncertainty matrix. In the present case, these matrices are written as

$$\mathbf{m}(s) = \left[\begin{array}{c|c}\mathbf{m}_{1,1}(s) & \mathbf{m}_{1,2}(s)\\ \hline \mathbf{m}_{2,1}(s) & m_{2,2}(s)\end{array}\right], \tag{50}$$

$$\boldsymbol{\delta}(s) = \mathrm{diag}[\tilde{\kappa}, \tilde{\alpha}, \tilde{\beta}, \tilde{\vartheta}(s), \tilde{\xi}], \tag{51}$$

where

$$\mathbf{m}_{1,1}(s) = \frac{1}{D(s)}\begin{bmatrix} \alpha\mathrm{e}^{-s\tau} & \mathrm{e}^{-s\tau} & \mathrm{e}^{-s\tau} & 2 & 1\\ \xi s^3 + s^2 + \beta s\mathrm{e}^{-s\tau} & -(\kappa+s)\mathrm{e}^{-s\tau} & (\kappa+s)\mathrm{e}^{-s\tau} & 2(\kappa+s) & s+\kappa\\ -\alpha s\mathrm{e}^{-s\tau} & -s\mathrm{e}^{-s\tau} & s\mathrm{e}^{-s\tau} & 2s & s\\ \alpha s^3(1+\xi s)\mathrm{e}^{-s\tau} & s^3(1+\xi s)\mathrm{e}^{-s\tau} & s^3(1+\xi s)\mathrm{e}^{-s\tau} & s\mathrm{e}^{-s\tau}c(s) - s^2(1+\xi s) & \mathrm{e}^{-s\tau}sc(s)\\ \mathrm{e}^{-s\tau}s^3\alpha & \mathrm{e}^{-s\tau}s^3 & \mathrm{e}^{-s\tau}s^3 & -2s^3 & -s^3 \end{bmatrix}, \tag{52}$$

$$\mathbf{m}_{1,2}(s) = \frac{1}{D(s)}\begin{bmatrix} s + \alpha\mathrm{e}^{-s\tau} + s^2\xi\\ \kappa s - \beta s\mathrm{e}^{-s\tau} + s^2\kappa\xi\\ \xi s^3 + s^2 + \alpha s\mathrm{e}^{-s\tau}\\ (\kappa\alpha s^2 + \beta s^3)\mathrm{e}^{-s\tau}(1+\xi s)\\ \mathrm{e}^{-s\tau}s^2(s\beta + \alpha\kappa)\end{bmatrix}, \tag{53}$$

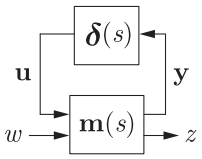

FIG. 7

$\mathbf{m} - \boldsymbol{\delta}$ uncertain interconnection structure.

$$\mathbf{m}_{2,1}(s) = \frac{1}{D(s)}\begin{bmatrix}\alpha s\mathrm{e}^{-s\tau} & s\mathrm{e}^{-s\tau} & s\mathrm{e}^{-s\tau} & -2s & -s\end{bmatrix}, \tag{54}$$

$$\mathbf{m}_{2,2}(s) = \frac{1}{D(s)}(\kappa\alpha + \beta s)\mathrm{e}^{-s\tau}, \tag{55}$$

moreover $D(s)$ is the characteristic function defined in Eq. (9) and $c(s) = s(\alpha+\beta) + \alpha\kappa$ is introduced for convenience. This is called the $\mathbf{m} - \boldsymbol{\delta}$ uncertain interconnection structure that can be graphically represented by the block diagram in Fig. 7; see Ref. [28].

The transfer function between the input w and output z involves the uncertainty matrix $\boldsymbol{\delta}(s)$. The solution can be expressed using the upper linear fractional transformation $\mathcal{F}_\mathrm{u}$ (upper LFT) as

$$\begin{aligned}\mathcal{F}_\mathrm{u}(\mathbf{m}(s), \boldsymbol{\delta}(s)) &:= \underbrace{m_{2,2}(s)}_{G_{i+1,i}(s)} + \underbrace{\mathbf{m}_{2,1}(s)\boldsymbol{\delta}(s)(\mathbf{I} - \mathbf{m}_{1,1}(s)\boldsymbol{\delta}(s))^{-1}\mathbf{m}_{1,2}(s)}_{\tilde{G}_{i+1,i}(s)} \\ &= \frac{((\kappa+\tilde{\kappa})(\alpha+\tilde{\alpha}) + (\beta+\tilde{\beta})s)\mathrm{e}^{-s\tau}\frac{1-s\tilde{\vartheta}(s)}{1+s\tilde{\vartheta}(s)}}{(\xi+\tilde{\xi})s^3 + s^2 + ((\kappa+\tilde{\kappa})(\alpha+\tilde{\alpha}) + (\alpha+\tilde{\alpha}+\beta+\tilde{\beta})s)\mathrm{e}^{-s\tau}\frac{1-s\tilde{\vartheta}(s)}{1+s\tilde{\vartheta}(s)}},\end{aligned} \tag{56}$$

under the condition that

$$\det(\mathbf{I} - \mathbf{m}_{1,1}(s)\boldsymbol{\delta}(s)) \neq 0. \tag{57}$$

One can show that this condition results the perturbed characteristic equation, and therefore, a necessary condition for robust plant stability. Note that Eq. (56) is equivalent to Eq. (39) including the Rekasius substitution.

Recall that the string stability criterion (35), similarly, the perturbed transfer function (56), needs to satisfy

$$1 - \mathcal{F}_\mathrm{u}(\mathbf{m}(\mathrm{i}\omega), \boldsymbol{\delta}(\mathrm{i}\omega))\delta^\mathrm{c} \neq 0, \quad \forall\omega > 0 \tag{58}$$

and for any complex number $\delta^\mathrm{c} \in \mathbb{C}$, $|\delta^\mathrm{c}| < 1$. Using the Schur formula (see Ref. [36]), we rewrite Eqs. (57), (58) for $s = \mathrm{i}\omega$ as

$$\det\left(\begin{bmatrix}\mathbf{I} & \mathbf{0}\\ \mathbf{0} & 1\end{bmatrix} - \begin{bmatrix}\mathbf{m}_{1,1}(\mathrm{i}\omega) & \mathbf{m}_{1,2}(\mathrm{i}\omega)\\ \mathbf{m}_{2,1}(\mathrm{i}\omega) & m_{2,2}(\mathrm{i}\omega)\end{bmatrix}\begin{bmatrix}\boldsymbol{\delta}(\mathrm{i}\omega) & \mathbf{0}\\ \mathbf{0} & \delta^{\mathrm{c}}\end{bmatrix}\right) \neq 0. \tag{59}$$

In Eq. (59), the uncertainty matrix is not normalized. Let us introduce the weights $\rho_i(s)$ and normalized uncertainties $\delta_i^{\mathrm{r}} \in \mathbb{R}$, $|\delta_i^{\mathrm{r}}| < 1$, such that

$$\tilde{\kappa} = \rho_1\delta_1^{\mathrm{r}}, \quad \tilde{\alpha} = \rho_2\delta_2^{\mathrm{r}}, \quad \tilde{\beta} = \rho_3\delta_3^{\mathrm{r}}, \quad \tilde{\vartheta}(s) = \rho_4(s)\delta_4^{\mathrm{r}}, \quad \tilde{\xi} = \rho_5\delta_5^{\mathrm{r}}, \tag{60}$$

where δ_i represents a real parameter uncertainty. Then, Eq. (59) can be rewritten in a normalized form as

$$\det(\mathbf{I} - \hat{\mathbf{m}}(\mathrm{i}\omega)\hat{\boldsymbol{\delta}}) \neq 0, \tag{61}$$

where

$$\hat{\mathbf{m}}(\mathrm{i}\omega) = \begin{bmatrix}\mathbf{m}_{1,1}(\mathrm{i}\omega)\mathbf{r}(\mathrm{i}\omega) & \mathbf{m}_{1,2}(\mathrm{i}\omega)\\ \mathbf{m}_{2,1}(\mathrm{i}\omega)\mathbf{r}(\mathrm{i}\omega) & m_{2,2}(\mathrm{i}\omega)\end{bmatrix}, \tag{62}$$

$$\mathbf{r}(\mathrm{i}\omega) = \mathrm{diag}[\rho_1, \rho_2, \rho_3, \rho_4(\mathrm{i}\omega), \rho_5], \tag{63}$$

$$\hat{\boldsymbol{\delta}} = \mathrm{diag}[\delta_1^{\mathrm{r}}, \delta_2^{\mathrm{r}}, \delta_3^{\mathrm{r}}, \delta_4^{\mathrm{r}}, \delta_5^{\mathrm{r}}, \delta^{\mathrm{c}}]. \tag{64}$$

Eq. (63) emphasizes that the weight of each parameter is constant, except for the time delay ($\rho_4 = \tilde{\vartheta}$), which varies with the frequency according to the Rekasius substitution.

In order to quantify the robustness of the system, we use the structured singular value (μ) analysis introduced by Doyle [28]. We define the μ-value of $\hat{\mathbf{m}}(\mathrm{i}\omega)$ as the inverse of the smallest $\bar{\sigma}(\hat{\boldsymbol{\delta}})$ when Eq. (61) fails at frequency ω, that is,

$$\mu(\omega) = \left(\min_{\hat{\boldsymbol{\delta}}}\{\bar{\sigma}(\hat{\boldsymbol{\delta}}):\ \det(\mathbf{I} - \hat{\mathbf{m}}(\mathrm{i}\omega)\hat{\boldsymbol{\delta}}) = 0\}\right)^{-1}, \tag{65}$$

where $\bar{\sigma}(\hat{\boldsymbol{\delta}})$ denotes the largest singular value of $\hat{\boldsymbol{\delta}}$. When Eq. (61) holds regardless of the perturbation values in $\hat{\boldsymbol{\delta}}$, we have $\mu(\omega) = \infty$, while if Eq. (61) is not satisfied for any perturbation structure, then $\mu(\omega) = 0$. As $\mu(\omega)$ increases, a smaller perturbation value in $\hat{\boldsymbol{\delta}}$ may lead to a singular $(\mathbf{I} - \hat{\mathbf{m}}(\mathrm{i}\omega)\hat{\boldsymbol{\delta}})$ and results in string instability. Therefore, the condition for robust string stability against bounded parameter variation is

$$\mu(\omega) < 1, \quad \forall\omega > 0, \tag{66}$$

similarly to the head-to-tail string stability Eq. (34).

Note that μ cannot be computed directly using Eq. (65), since the optimization problem is not convex in general and may have multiple local extrema [37]. However, if we are interested in finding upper and/or lower bounds, several alternative formulations have been developed [28,37–39]. In this work, we use the `mussv` function in MATLAB μ-Analysis and Synthesis Toolbox to obtain the upper and lower bounds of μ [40].

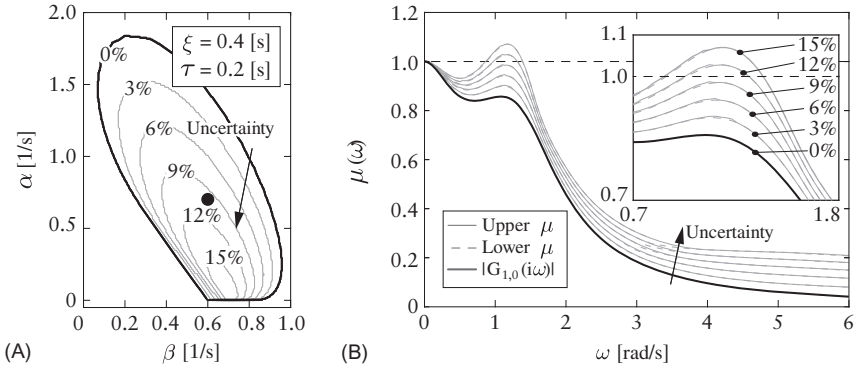

FIG. 8

(A) Robust stability charts in the plane (β, α) for $\kappa = 0.6$ [1/s], $\tau = 0.2$ [s], $\xi = 0.4$ [s] with uncertainties 0%, 3%, 6%, 9%, 12%, and 15% in κ, ξ, and τ (0% in α and β). *Black curves* indicate the nominal string stable boundary (0% uncertainty) and *dark gray curves* indicate the robust string stable boundaries. (B) The nominal transfer function $|G_{i+1,i}(\mathrm{i}\omega)|$ curve (*thick black*) and $\mu(\omega)$ curves (*thin gray*) for parameter point $(\beta, \alpha) = (0.6, 0.7)$ [1/s] marked by a *black dot* in panel (A).

As an example, a robust string stability diagram is presented in Fig. 8. To demonstrate the sensitivity of the string stable domain, we chose the parameters $\kappa = 0.6$ [1/s], $\tau = 0.2$ [s], $\xi = 0.4$ [s], as shown in the middle panel in Fig. 2. Panel (A) shows the contraction of the robust string stable region as the uncertainty increases from 0% to 15% in parameters κ, τ, and ξ, while panel (B) plots the μ-bounds corresponding to control gains $\alpha = 0.6$ [1/s] and $\beta = 0.7$ [1/s] marked as a black dot. Note that when the uncertainty in the parameters are set to zero, that is, $\mathbf{r}(\mathrm{i}\omega) = \mathbf{0}$, then the robust string stable condition (61) reduces to the nominal string stable condition (58), which is satisfied only if $\delta^{\mathrm{c}} = G_{i+1,i}(\mathrm{i}\omega)^{-1}$. In this case one obtains $\mu(\omega) = |G_{i+1,i}(\mathrm{i}\omega)|$ by definition from Eq. (65).

3.2 Robust connected cruise control design

In order to demonstrate the applicability of the method developed here, we present a case study for the connected vehicle system consisting of a connected automated vehicle and three human-driven cars with uncertainty, that is, $n = 3$ in Eq. (27) as shown in Fig. 9A. The schematic block diagram with uncertainties is presented in Fig. 9B, which is the extension of Fig. 4B. While the nominal transfer function matrix is given in Eq. (36), we assume each parameter in vehicles 2 and 1 have certain levels of uncertainty and compute the robust string stable regions in the $(B_{2,0}, B_{3,0})$-plane for different values of $A_{1,0}$ and $B_{1,0}$.

In order to construct a connected uncertainty structure, we need to include the uncertain model for each vehicle that might be different. Let us use upper indices

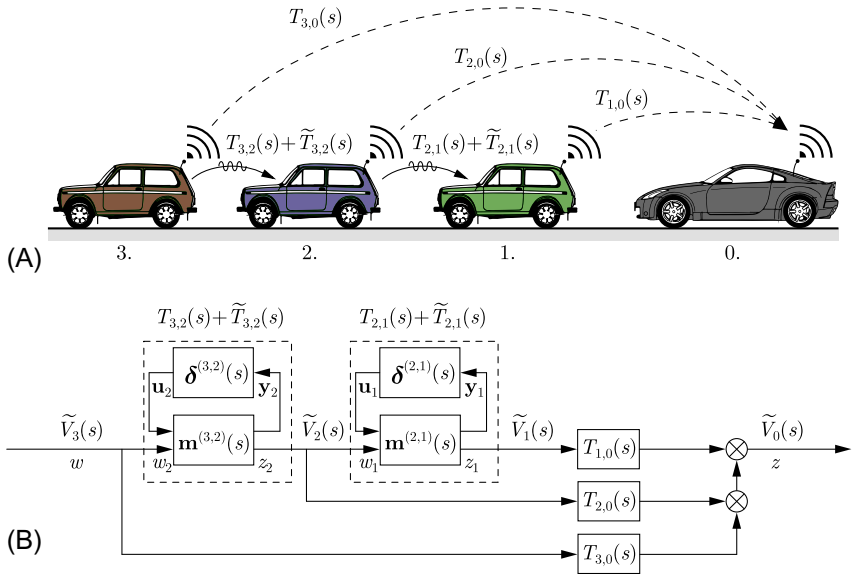

FIG. 9

Example configuration with uncertainties: (A) connectivity topology and (B) block diagram.

(3, 2) and (2, 1) to denote the links between vehicles 3–2 and 2–1. The corresponding system of equations for each vehicle read

$$\mathbf{y}_1 = \mathbf{m}_{1,1}^{(2,1)}(s)\mathbf{u}_1 + \mathbf{m}_{1,2}^{(2,1)}(s)w_1, \tag{67}$$

$$\mathbf{y}_2 = \mathbf{m}_{1,1}^{(3,2)}(s)\mathbf{u}_2 + \mathbf{m}_{1,2}^{(3,2)}(s)w_2, \tag{68}$$

$$z_1 = \mathbf{m}_{2,1}^{(2,1)}(s)\mathbf{u}_1 + \mathbf{m}_{2,2}^{(2,1)}(s)w_1, \tag{69}$$

$$z_2 = \mathbf{m}_{2,1}^{(3,2)}(s)\mathbf{u}_2 + \mathbf{m}_{2,2}^{(3,2)}(s)w_2, \tag{70}$$

$$z = T_{1,0}(s)z_1 + T_{2,0}(s)z_2 + T_{3,0}(s)w_2, \tag{71}$$

$$w_1 = z_2, \tag{72}$$

$$w_2 = w. \tag{73}$$

Note that here we have $w = \tilde{V}_3(s)$ and $z = \tilde{V}_0(s)$. After simplifications with $\mathbf{m}_{2,2}^{(2,1)}(s) = T_{2,1}(s)$ and $\mathbf{m}_{2,2}^{(3,2)}(s) = T_{3,2}(s)$, the solution for Eqs. (67)–(73) directly yields

$$\begin{bmatrix} \mathbf{y}_1 \\ \mathbf{y}_2 \\ z \end{bmatrix} = \mathbf{M}(s) \begin{bmatrix} \mathbf{u}_1 \\ \mathbf{u}_2 \\ w \end{bmatrix}, \tag{74}$$

where the interconnection structure is given by

$$\mathbf{M}(s) = \left[\begin{array}{cc|c} \mathbf{m}_{1,1}^{(2,1)}(s) & \mathbf{m}_{1,2}^{(2,1)}(s)\mathbf{m}_{2,1}^{(3,2)}(s) & \mathbf{m}_{12}^{(2,1)}(s)T_{3,2}(s) \\ \mathbf{0} & \mathbf{m}_{1,1}^{(3,2)}(s) & \mathbf{m}_{1,2}^{(3,2)}(s) \\ \hline \mathbf{m}_{2,1}^{(2,1)}(s)T_{1,0}(s) & \mathbf{m}_{2,1}^{(3,2)}(s)(T_{2,0}(s) + T_{1,0}(s)T_{2,1}(s)) & G_{3,0}(s) \end{array}\right], \quad (75)$$

and the weight matrix of the corresponding uncertainties reads

$$\mathbf{R}(s) = \begin{bmatrix} \mathbf{r}^{(2,1)}(s) & \mathbf{0} \\ \mathbf{0} & \mathbf{r}^{(3,2)}(s) \end{bmatrix}. \quad (76)$$

With some generalizations, one can show that the structure of equations remains the same, that is,

$$\det(\mathbf{I} - \hat{\mathbf{M}}(\mathrm{i}\omega)\hat{\mathbf{\Delta}}) \neq 0, \quad (77)$$

where

$$\hat{\mathbf{M}}(\mathrm{i}\omega) = \begin{bmatrix} \mathbf{M}_{1,1}(\mathrm{i}\omega)\mathbf{R}(\mathrm{i}\omega) & \mathbf{M}_{1,2}(\mathrm{i}\omega) \\ \mathbf{M}_{2,1}(\mathrm{i}\omega)\mathbf{R}(\mathrm{i}\omega) & M_{2,2}(\mathrm{i}\omega) \end{bmatrix}, \quad (78)$$

$$\hat{\mathbf{\Delta}} = \mathrm{diag}[\delta_1^{\mathrm{r}}, \ldots, \delta_{10}^{\mathrm{r}}, \delta^{\mathrm{c}}]. \quad (79)$$

Here, 10 corresponds to the $5 + 5$ independent parameters of vehicles 1 and 2.

Again, the computation of μ-values are performed by the MATLAB toolbox using the `mussv` function. The results are presented in Fig. 10A, where we assumed that each parameter of each vehicle is perturbed by the same percentage of their nominal value, that is, α_i, β_i, κ_i, τ_i, and ξ_i has identical relative uncertainty. The nominal human driver parameters are $\kappa_i = 0.8$ [1/s], $\alpha_i = 0.25$ [1/s], $\beta_i = 0.5$ [1/s], $\tau_i = 0.3$ [s], and $\xi_i = 0.5$ [s] (same for both vehicles for simplicity), while the fixed parameters of the connected automated vehicle are $\kappa_0 = 0.6$ [1/s], $\sigma = \sigma_{1,0} = \sigma_{2,0} = \sigma_{3,0} = 0.1$ [s], and $\xi_0 = 0.5$ [s]. The same set of parameters were used in the simulations in Section 2.2, Fig. 5. In this configuration, human-driven vehicles are string unstable, but head-to-tail string stability can be guaranteed by appropriate selection of the gains of the connected automated vehicle. The subplots in Fig. 10A show how the uncertain parameters (10 in total) affect the robust stable domain of control parameters $(A_{1,0}, B_{1,0}, B_{2,0}, B_{3,0})$. One of the most robust parameter combination for realizable gain combinations is located at $(0.4, 0.2, 0.3, 0.3)$ [1/s].

For this point, some $\mu(\omega)$ curves are presented in Fig. 10B for different uncertainty levels. The curves show that the upper-lower bounds are sufficiently tight, therefore, the robust boundaries obtained by the numerical method are close to the real robust boundaries. The μ-curves also show that at least 20% robustness can be guaranteed with the selected control gains.

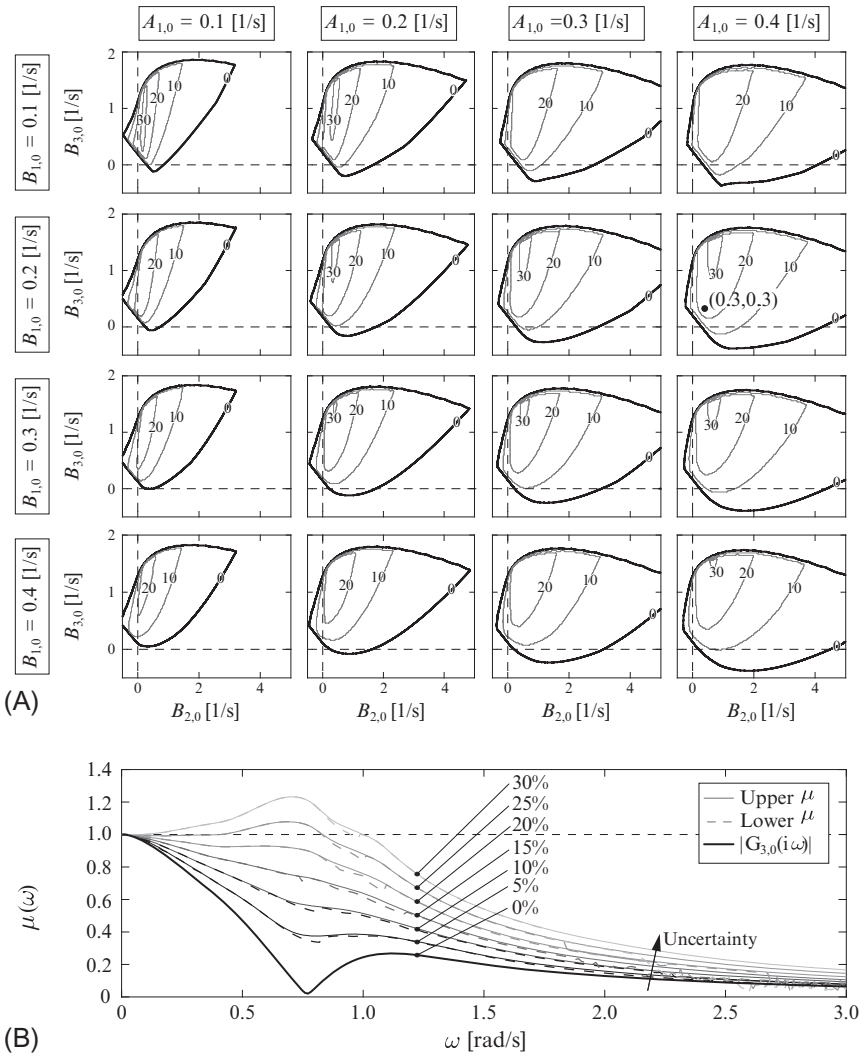

FIG. 10

(A) Robust string stability charts in the $(B_{2,0}, B_{3,0})$ plane for different values of $A_{1,0}$ and $B_{1,0}$, when using uncertainties 10–20–30%. (B) μ-curves for different levels of uncertainty at parameter point $(A_{10}, B_{10}, B_{20}, B_{30}) = (0.4, 0.2, 0.3, 0.3)$ [1/s].

4 Conclusion

In this chapter, we applied the structured singular value analysis to investigate the influences of uncertain human car-following parameters on string stability of

connected cruise controllers. In particular, the uncertain time delays were handled using the Rekasius substitution, so that the robust bounds on head-to-tail string stability remained tight. We demonstrated through case studies that these robustness results could be used to design connected automated vehicles that reject traffic perturbations well and improves performance of traffic flow despite uncertain human car-following behavior.

Acknowledgment

This work is supported by the ÚNKP-17-3-I. The research reported in this paper was supported by the Higher Education Excellence Program of the Ministry of Human Capacities in the frame of Artificial intelligence research area of Budapest University of Technology and Economics (BME FIKP-MI). New National Excellence Program of the Ministry of Human Capacities.

References

[1] P.I. Labuhn, W.J. Chundrlik, Adaptive cruise control, 1995, US Patent 5,454,442.
[2] J. Vander Werf, S. Shladover, M. Miller, N. Kourjanskaia, Effects of adaptive cruise control systems on highway traffic flow capacity, Transp. Res. Rec. J. Transp. Res. Board 1800 (2002) 78–84.
[3] S. Shladover, D. Su, X.-Y. Lu, Impacts of cooperative adaptive cruise control on freeway traffic flow, Transp. Res. Rec. J. Transp. Res. Board 2324 (2012) 63–70.
[4] P.A. Barber, G.H. Engelman, P.J. King, M.J. Richardson, Adaptive Cruise Control System and Methodology, Including Control of Inter-Vehicle Spacing, 2009, EP Patent 1,008,482.
[5] V. Milanes, J. Alonso, L. Bouraoui, J. Ploeg, Cooperative maneuvering in close environments among cybercars and dual-mode cars, IEEE Trans. Intell. Transp. Syst. 12 (1) (2011) 15–24.
[6] M. Wang, W. Daamen, S.P. Hoogendoorn, B. van Arem, Rolling horizon control framework for driver assistance systems. Part II: cooperative sensing and cooperative control, Transp. Res. C 40 (2014) 290–311.
[7] J. Ploeg, N. van de Wouw, H. Nijmeijer, $\mathcal{L}_p$ string stability of cascaded systems: application to vehicle platooning, IEEE Trans. Control Syst. Technol. 22 (2) (2014) 786–793.
[8] V. Milanes, S.E. Shladover, Modeling cooperative and autonomous adaptive cruise control dynamic responses using experimental data, Transp. Res. C Emerg. Technol. 48 (2014) 285–300.
[9] B. van Arem, C.J.G. van Driel, R. Visser, The impact of cooperative adaptive cruise control on traffic-flow characteristics, IEEE Trans. Intell. Transp. Syst. 7 (4) (2006) 429–436.
[10] J. Ploeg, D. Shukla, N. van de Wouw, H. Nijmeijer, Controller synthesis for string stability of vehicle platoons, IEEE Trans. Intell. Transp. Syst. 15 (2) (2014) 845–865.
[11] J. Lioris, R. Pedarsani, F.Y. Tascikaraoglu, P. Varaiya, Platoons of connected vehicles can double throughput in urban roads, Transp. Res. C Emerg. Technol. 77 (2017) 292–305.

[12] S.E. Li, R. Li, J. Wang, X. Hu, B. Cheng, K. Li, Stabilizing periodic control of automated vehicle platoon with minimized fuel consumption, IEEE Trans. Transp. Electr. 3 (1) (2017) 259–271.
[13] E. van Nunen, M.R.J.A.E. Kwakkernaat, J. Ploeg, B.D. Netten, Cooperative competition for future mobility, IEEE Trans. Intell. Transp. Syst. 13 (3) (2012) 1018–1025.
[14] C. Englund, L. Chen, J. Ploeg, E. Semsar-Kazerooni, A. Voronov, H.H. Bengtsson, J. Didoff, The grand cooperative driving challenge 2016: boosting the introduction of cooperative automated vehicles, IEEE Wirel. Commun. 23 (4) (2016) 146–152.
[15] S.E. Shladover, C. Nowakowski, X.-Y. Lu, R. Ferlis, Cooperative adaptive cruise control definitions and operating concepts, Transp. Res. Rec. J. Transp. Res. Board 2489 (2015) 145–152.
[16] G. Orosz, Connected cruise control: modeling, delay effects, and nonlinear behaviour, Veh. Syst. Dyn. 54 (8) (2016) 1147–1176.
[17] L. Zhang, G. Orosz, Motif-based analysis of connected vehicle systems: delay effects and stability, IEEE Trans. Intell. Transp. Syst. 17 (6) (2016) 1638–1651.
[18] J.I. Ge, G. Orosz, Dynamics of connected vehicle systems with delayed acceleration feedback, Transp. Res. C 46 (2014) 46–64.
[19] S.S. Avedisov, G. Orosz, Analysis of connected vehicle networks using network-based perturbation techniques, Nonlinear Dyn. 89 (3) (2017) 1651–1672.
[20] J.I. Ge, G. Orosz, D. Hajdu, T. Insperger, J. Moehlis, To delay or not to delay—stability of connected cruise control, in: G. Orosz, T. Ersal, T. Insperger (Eds.), Time Delay Systems—Theory, Numerics, Applications and Experiments, Advances in Delays and Dynamics, vol. 7, Springer, 2016, pp. 263–282.
[21] F. Gao, S.E. Li, Y. Zheng, D. Kum, Robust control of heterogeneous vehicular platoon with uncertain dynamics and communication delay, IET Intell. Transp. Syst. 10 (7) (2016) 503–513.
[22] S.E. Li, F. Gao, K. Li, L.Y. Wang, K. You, D. Cao, Robust longitudinal control of multi-vehicle systems—a distributed H-infinity method, IEEE Trans. Intell. Transp. Syst. 19 (9) (2018) 2779–2788.
[23] Y. Zheng, S.E. Li, K. Li, W. Ren, Platooning of connected vehicles with undirected topologies: robustness analysis and distributed H-infinity controller synthesis, IEEE Trans. Intell. Transp. Syst. 19 (5) (2018) 1353–1364.
[24] L. Zhang, J. Sun, G. Orosz, Hierarchical design of connected cruise control in the presence of information delays and uncertain vehicle dynamics, IEEE Trans. Control Syst. Technol. 26 (1) (2018) 139–150.
[25] M. di Bernardo, A. Salvi, S. Santini, Distributed consensus strategy for platooning of vehicles in the presence of time varying heterogeneous communication delays, IEEE Trans. Intell. Transp. Syst. 16 (1) (2015) 102–112.
[26] W.B. Qin, G. Orosz, Scalable stability analysis on large connected vehicle systems subject to stochastic communication delays, Transp. Res. C Emerg. Technol. 83 (2017) 39–60.
[27] Y. Zhou, S. Ahn, M. Chitturi, D.A. Noyce, Rolling horizon stochastic optimal control strategy for ACC and CACC under uncertainty, Transp. Res. C Emerg. Technol. 83 (2017) 61–76.
[28] J.C. Doyle, Analysis of feedback systems with structured uncertainties, IEE Proc. D Control Theory Appl. 129 (6) (1982) 242–250.
[29] K. Zhou, J.C. Doyle, Essentials of Robust Control, Prentice Hall Modular Series, Prentice Hall, 1998.

[30] Y. Zheng, S.E. Li, J. Wang, D. Cao, K. Li, Stability and scalability of homogeneous vehicular platoon: study on the influence of information flow topologies, IEEE Trans. Intell. Transp. Syst. 17 (1) (2016) 14–26.
[31] J.I. Ge, G. Orosz, Dynamics of connected vehicle systems with delayed acceleration feedback, Transp. Res. C 46 (2014) 46–64.
[32] D. Helbing, Traffic and related self-driven many-particle systems, Rev. Mod. Phys. 73 (2001) 1067–1141.
[33] P. Seiler, A. Pant, K. Hedrick, Disturbance propagation in vehicle strings, IEEE Trans. Autom. Control 49 (10) (2004) 1835–1841.
[34] N. Olgac, R. Sipahi, An exact method for the stability analysis of time-delayed linear time-invariant (LTI) systems, IEEE Trans. Autom. Control 47 (5) (2002) 793–797.
[35] F. Lescher, C. Roos, Robust stability of time-delay systems with structured uncertainties: a μ-analysis based algorithm, in: 2011 50th IEEE Conference on Decision and Control and European Control Conference, 2011, pp. 4955–4960.
[36] C. Scherer, Theory of Robust Control, TU Delft, 2001.
[37] P.M. Young, M.P. Newlin, J.C. Doyle, μ Analysis with real parametric uncertainty, in: Proceedings of the 30th IEEE Conference on Decision and Control, vol. 2, 1991, pp. 1251–1256.
[38] A. Packard, J.C. Doyle, The complex structured singular value, Automatica 29 (1) (1993) 71–109.
[39] M.K.H. Fan, A.L. Tits, J.C. Doyle, Robustness in the presence of mixed parametric uncertainty and unmodeled dynamics, IEEE Trans. Autom. Control 36 (1991) 25–38.
[40] G. Balas, J.C. Doyle, K. Glover, A. Packard, R. Smith, μ-Analysis and Synthesis Toolbox for Use With Matlab User's Guide, The MathWorks Inc., 1993.